Journal of Materials Chemistry C

Accepted Manuscript

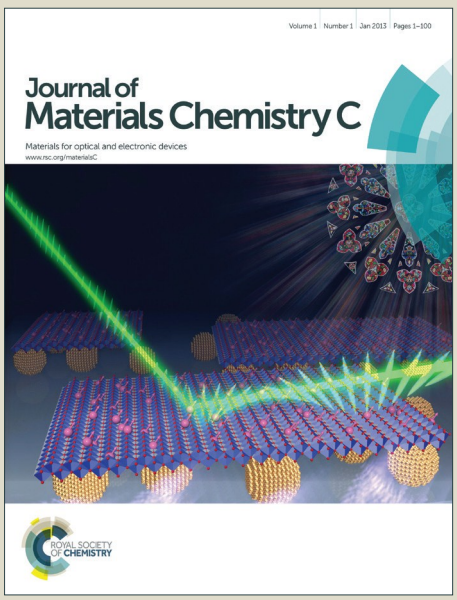

ROYAL SOCIETY OF CHEMISTRY

www.rsc.org/materialsC

Journal of Materials Chemistry C

ARTICLE

Photocurrent Enhancement of Porphyrin Molecules over a Wide-Wavelength Region Based on Combined Use of Silver Nanoprisms with Different Aspect Ratios

Received 00th January 20xx,
Accepted 00th January 20xx

DOI: 10.1039/x0xx00000x

www.rsc.org/

Kosuke Sugawa,*[a] Naoto Takeshima,[a] Koji Uchida,[a] Hironobu Tahara,[b] Shota Jin,[a] Natsumi Tsunenari,[a] Tsuyoshi Akiyama,[c] Yasuyuki Kusaka,[d] Nobuko Fukuda,[d] Hirobumi Ushijima,[d] Yuji Tsuchido,[e] Takeshi Hashimoto,[e] Takashi Hayashita,[e] and Joe Otsuki[a]

We succeeded in controlling the wavelength range in which the photocurrent of porphyrin is enhanced by tuning as well as expanding the wavelength ranges in which the localized surface plasmon resonance (LSPR) occurs. We fabricated photoelectric conversion systems consisting of 5,10,15,20-tetrakis(*p*-carboxyphenyl)porphyrin (TCPP) and silver nanoprisms with small (SAgPRs) and large (LAgPRs) aspect ratios as plasmonic nano-antennae. Their photocurrents were much larger than those from TCPP-modified Ag planar electrodes at the specific wavelengths corresponding to their LSPR bands (SAgPRs: 460–610 nm; LAgPRs: 610–690 nm). The maximum enhancement factors (EFs) for the SAgPRs and the LAgPRs were 37 and 35, respectively. In order to enhance the photocurrents, we expanded the LSPR bands by the combined use of SAgPRs and LAgPRs. The system consisting of the mixture (MAgPRs) showed enhancement of the photocurrent over the entire Q-band region (480-690 nm). Finally, the total EFs of the photocurrents were evaluated by irradiation with AM1.5G sunlight through a long-pass filter of 480 nm and the results revealed that the EFs were in the order of MAgPRs > SAgPRs > LAgPRs. Furthermore, the system showed stability without loss of the enhancement property for at least 10 min under the solar irradiation.

1. Introduction

The development of highly-efficient organic photoelectric conversion systems driven by visible light is of significance for application in areas such as organic solar cells,[1] artificial photosynthesis,[2] and photoelectrochemical biosensing,[3] as well as for elucidating fundamental photochemical reactions. Porphyrins are particularly attractive photofunctional molecules in this context, due to their structural similarity to chlorophylls in natural photosynthesis and their favorable optoelectronic properties.[4,5] However, the absorption coefficient of the Q-band (~480–690 nm; ~10^4 M^{-1} cm^{-1}) that cover a wide range of visible spectrum is significantly smaller than that of the Soret band (~420 nm; >10^5 M^{-1} cm^{-1}) in the UV region.[6] Therefore, in order to develop highly efficient photoelectric conversion systems based on porphyrin molecules, it is necessary to enhance the conversion efficiency over the wide Q-band region. The introduction of "organic light harvesting antennae" into the system, which led to the additional generation of energy-transfer-mediated photocurrents within the desired wavelength region, has been investigated in an effort to resolve this issue.[7,8] More recently, some research groups have suggested that the plasmonic metal nanostructures can be used for the light harvesting. The photocurrents from organic dye molecules positioned adjacent to the metal nanostructures (metal species: Au and Ag) were enhanced by the effect of the localized surface plasmon resonance (LSPR) occurring on the surface of the nanostructures.[9-23] This enhancement was attributed to the efficient electronic excitation of the dye molecules, which is induced by generation of confined strong local electromagnetic fields, upon the LSPR excitation. In other words, the plasmonic nanostructures were capable of acting as "light-harvesting plasmonic nano-antennae" in the organic photoelectric conversion systems.

We have previously reported the enhancement of photocurrent from self-assembled monolayers (SAMs) of a

[a] College of Science and Technology, Nihon University, Chiyoda, Tokyo 101-8308, Japan.
[b] Division of Chemistry and Materials Science, Graduate School of Engineering, Nagasaki University, Nagasaki 852-8521, Japan.
[c] Department of Materials Science, School of Engineering, The University of Shiga Prefecture, Hikone, Shiga 522-8583, Japan.
[d] Flexible Electronics Research Center, National Institute of Advanced Industrial Science and Technology (AIST), Tsukuba, Ibaraki 305-8565, Japan
[e] Department of Materials and Life Sciences, Faculty of Science and Technology, Sophia University, Chiyoda-ku, Tokyo 102-8554, Japan
† E-mail: sugawa.kosuke@nihon-u.ac.jp
Electronic Supplementary Information (ESI) available: Detailed experimental procedures of preparation of SAgPRs and LAgPRs covered with silica layers and Figure S1-S5. See DOI: 10.1039/x0xx00000x

porphyrin derivative immobilized on two-dimensional Au nanoparticle assemblies,[9,11] Au nanocorals,[10] and regularly arrayed Au nanostructures.[12] Ikeda et al. have reported photocurrent enhancement of porphyrin–ferrocene molecules placed within the gap between gold nanoparticles and gold planar plate.[15,21] The LSPR from the Au nanostructures is generated effectively in a wavelength region above ~530 nm, where the imaginary part of the dielectric constant of Au is sufficiently small.[24,25] However, plasmon hybridization between two or more gold nanoparticles, which can generate much stronger local electromagnetic fields (hot spots), causes the LSPR peak to be red-shifted to longer wavelength regions.[26] Therefore, it is difficult for Au LSPR to efficiently enhance the photocurrents over the whole Q-band region. Indeed, previous studies employing Au LSPR have demonstrated an effective enhancement of the photocurrent from porphyrin only above 600 nm.[9,10,15,21] Plasmonic Ag nanostructures have advantages over Au nanostructures for the development of highly efficient photoelectric conversion systems, due to the following reasons. First, the confined local electromagnetic fields generated at Ag nanostructured surfaces are generally much stronger than those for Au.[25-27] It is therefore highly possible that the photocurrents from the dye molecules adjacent to the Ag nanostructures could be significantly enhanced. Second, Ag LSPR occurs over a wider visible wavelength region (longer than ~400 nm) than that by Au LSPR, which may cover the whole Q-band region of porphyrin.[25,26] Therefore, the Ag LSPR has a great potential to improve the photocurrent of porphyrin over a wide region. Despite these advantages, however, reports for the development of photoelectric conversion systems based on the plasmonic Ag nanostructures are few.[16-19,23] This could be due to the difficulty in handling Ag nanostructures (nanoparticles) and/or due to the instability of Ag nanoparticles upon light irradiation due to photocorrosion.[19,23] As a consequence, the effective enhancement of photocurrent signals from organic chromophores close to Ag nanoparticles by their LSPR has not been achieved.

In this study, we report the improvement of photocurrent over a wide Q band region above 480 nm based on the utilization of "plasmonic Ag nano-antennae" and the sophisticated control and expansion of the Ag LSPR band. In order to achieve this, Ag triangular nanoplates (Ag nanoprisms; AgPRs) were chosen because the local electromagnetic fields generated on the corner of the AgPRs are expected to be stronger by an order of magnitude than those from regular spherical silver nanoparticles.[27] Also, the plasmon frequency can be tuned over a wide range (from visible to near-infrared region) by adjusting the aspect ratio, *i.e.* the ratio of its edge length to its thickness.[28] In addition, AgPRs has sometimes been applied to plasmonic thin donor/acceptor photovoltaic films.[29-34] In this study, we first evaluated the effect of two kinds of AgPRs with different aspect ratios on the photocurrent enhancement from the nearby porphyrin molecules. Next, we fabricated photoelectric conversion systems consisting of porphyrin and a mixture of these AgPRs, which generate the LSPR at different wavelength regions. The combined use of these AgPRs enabled the LSPR bands to cover the whole Q-band region. As a result, we succeeded in effectively enhancing the photocurrent over the entire Q-band region.

2. Experimental

2.1. Materials

Deionized water (resistivity: 18.2 MΩ·cm) obtained from a Milli-Q water purification system, was used for the preparation of all aqueous solutions. Sodium tetrahydroborate ($NaBH_4$, Wako Pure Chemicals), trisodium citrate dihydrate (Kanto Chemicals), silver nitrate ($AgNO_3$, Wako Pure Chemicals), sodium hydroxide (NaOH, Kanto Chemicals), poly(ethylene imine) (PEI; MW = 50000-100000, Sigma Aldrich), ammonium solution (NH_3, 28%, Kanto Chemicals), hydrogen peroxide solution (H_2O_2, 30%, Kanto Chemicals), 16-mercaptohexadecanoic acid (MHA, Sigma Aldrich), poly(4-styrenesulfonic acid) sodium salt (PSS, Sigma Aldrich), titanium butoxide ($Ti(OBu)_4$, Wako Pure Chemicals), and 5,10,15,20-tetrakis(*p*-carboxyphenyl)porphyrin (TCPP, Wako Pure Chemicals) were used as received.

2.2. Preparation of colloidal solutions of AgPRs

Colloidal aqueous solutions of two kinds of AgPRs with different aspect ratios were prepared by modified photochemical growth methods.[35-37] First, a colloidal aqueous solution of seeds of Ag nanospheres was prepared by a modified reported procedure.[38] In brief, an aqueous solution of $AgNO_3$ (1 mM, 100 mL) was added to an aqueous solution (100 mL) of 0.2 mM of $NaBH_4$ and 5 mM of trisodium citrate under cooling in an ice bath, followed by stirring for 1 h. The average diameter of the resultant silver nanoparticles, which was estimated from their TEM images, was ~11 nm. Next, the pH of the obtained colloidal solution was adjusted to 11.2 by the addition of an aqueous solution of 0.2 M NaOH. This was followed by irradiation of the colloidal solutions for about 16 h by light-emitting diodes (LEDs) with center wavelengths of 470 nm and 550 nm, which resulted in the formation of AgPRs of smaller (SAgPRs) and larger (LAgPRs) aspect ratios, respectively.

2.3. Fabrication of photoelectric conversion systems consisting of AgPRs and TCPP

The fabrication of the photoelectric conversion systems consisting of the AgPRs (both SAgPRs and LAgPRs) and the TCPP molecules is shown in Scheme 1(A). An indium-tin-oxide (ITO) electrode (15 mm × 20 mm) was treated in a mixture of NH_3 aq.(28%)/H_2O_2 aq.(30%) (1/1 v/v) at 100 °C, then washed thoroughly with water, and dried in a stream of nitrogen. It was then immersed in an aqueous PEI solution (4.5 mg/mL) for 10 min and washed with water to make the surface positively charged.[16] Next, the electrode was immersed in a colloidal solution of the negatively-charged (derived from citric acid as a protecting agent) AgPRs (SAgPRs or LAgPRs) for 1 h, followed by washing with water, to produce the AgPRs-modified electrodes *via* electrostatic interaction (denoted as SAgPRs/ITO or LAgPRs/ITO). The electrode was then immersed

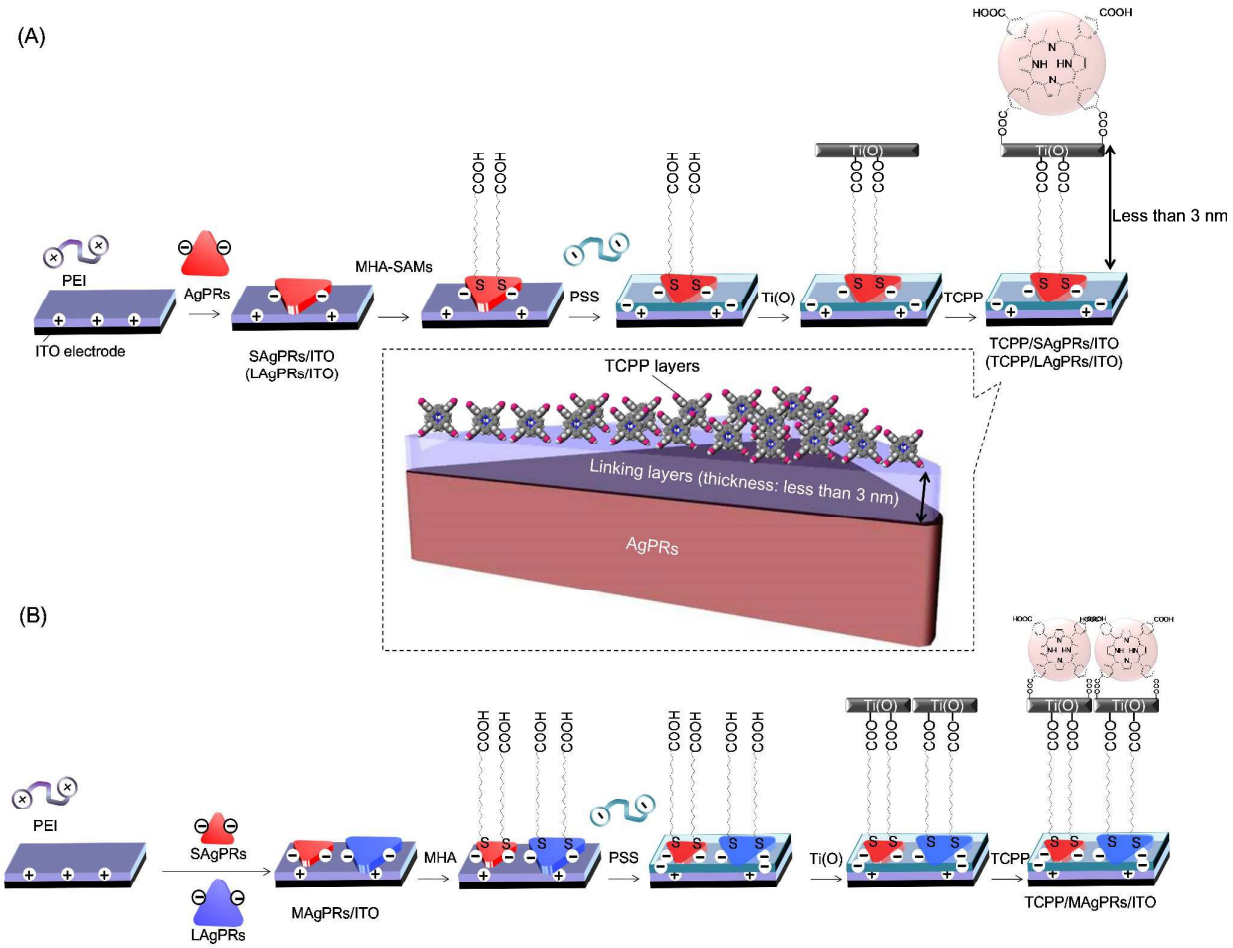

Scheme 1. Fabrication scheme of the photoelectric conversion systems comprised of TCPP and AgPRs by the layer-by-layer assembly technique. (A) Individual AgPRs (SAgPRs and LAgPRs) and (B) the mixture of SAgPRs and LAgPRs with different aspect ratios.

in an ethanol solution of MHA (1 mM) for 1 h, followed by washing with ethanol, to form the MHA SAMs on the surface of the AgPRs *via* strong bonding between the Ag atoms and the thiol.[39] This was followed by immersion of the electrode in an aqueous solution of PSS (4.2 mg/mL) for 10 min and then washing with water to make the PEI domains not covered with the AgPRs negatively charged. With this process, the adsorption of the negatively charged TCPP onto the PEI domains *via* electrostatic adsorption in the next step was largely suppressed. Finally, the TCPP was immobilized on the surface of the AgPRs by the surface sol-gel process.[40,41] The electrode was immersed in a toluene solution of $Ti(OBu)_4$ (0.1 M) for 10 min to achieve coordinate bonding of MHA with titanium oxide (Ti(O)), followed by washing with ethanol, and then dipping into water to generate surface hydroxyl groups by hydrolysis. The electrode was then immersed into an ethanol solution of TCPP (0.1 mM) for 10 min, followed by washing with ethanol and drying in a stream of nitrogen. The systems consisting of TCPP and the SAgPRs (or the LAgPRs) fabricated by these processes were denoted as TCPP/SAgPRs/ITO (or TCPP/LAgPRs/ITO).

The photoelectric conversion system based on the mixture (MAgPRs) of SAgPRs and LAgPRs was fabricated as shown in Scheme 1(B). Firstly, the PEI-modified ITO electrode was dipped for 1 h in a colloidal solution mixture of SAgPR aq./LAgPRs aq.=1/1 v/v, resulting in the formation of the MAgPRs-immobilized ITO electrode (MAgPRs/ITO). The rest of the procedure was the same as described for the fabrication of TCPP/SAgPRs(LAgPRs)/ITO, and the obtained electrode is denoted as TCPP/MAgPRs/ITO.

2.4. Fabrication of the photoelectric conversion systems consisting of a planar silver electrode and TCPP

A two-dimensional planar silver electrode with a mirror surface (AgP/ITO) was prepared by thermal deposition of Ag (thickness: 100 nm) onto the surface of an ITO electrode under high vacuum (1×10^{-6} Torr). The electrode was then immersed in an ethanol solution of MHA (1 mM) for 1 h, followed by washing with ethanol to form the MHA SAMs on the surface. TCPP was immobilized onto the surface of the AgP/ITO by the surface sol-gel process described above.

2.5. Estimation of the electromagnetic fields generated on the AgPRs

In order to analyze the electromagnetic field enhancement factor due to LSPR of AgPRs, finite difference time domain (FDTD) calculation were carried out by using the FullWAVE program suite (RSoft Design Group, Inc.). The dielectric function of silver used was obtained from the previous report by Rakic *et al.*[42] The refractive index of the background is set to 1.333 corresponding to water. The electromagnetic field of SAgPR and LAgPR was modeled as an isolated system.

2.6. Measurements

Absorption and extinction spectra were recorded on a JASCO V-630 spectrophotometer. Fluorescence excitation spectra were measured using a JASCO FP-6500 spectrofluorometer. Scanning electron microscopy (SEM) experiments were carried out employing a HITACHI S-4500 microscope. Transmission electron microscopy (TEM) images were obtained using a Hitachi HF-2000 system at an acceleration voltage of 200 kV. The atomic force microscope (AFM, tapping mode) measurements were conducted using LEXT-3000 (Shimadzu, Japan). Dynamic light scattering (DLS) measurements used to evaluate zeta potentials were carried out using a Zetasizer Nano ZS (Malvern Instruments Ltd, Malvern, Worcestershire, United Kingdom) at a wavelength of 633 nm. Photocurrent measurements were carried out in an aqueous solution of 0.1 M $NaClO_4$ containing 5 mM methyl viologen as an electron acceptor, using a home-made three-electrode photoelectrochemical cell with Ag|AgCl (sat. KCl aq.), platinum wire, and the TCPP/AgPRs (SAgPRs, LAgPRs, and MAgPRs)/ITO and TCPP/AgP/ITO as the reference, counter, and the working electrodes, respectively. Before the measurements, N_2 was bubbled through the solution for 2 h. Monochromatic light from a Xe lamp was used to irradiate the TCPP molecular layers. All photocurrents were measured at E = 0 V *vs.* Ag|AgCl and detected using a potentiostat (Huso HECS 318E).

3. Results and discussion

3.1. Morphological and optical characterization of AgPRs

The edge lengths of the SAgPRs and the LAgPRs were estimated to be 27 ± 3 and 44 ± 5 nm, respectively from the TEM images [Figure 1(A)]. Estimation of their thicknesses from the TEM images was difficult because the AgPRs were thin and, therefore, most of the obtained TEM images showed triangular front views of AgPRs. In order to estimate the thickness, the AgPRs were covered by silica shells of sufficient thickness by a chemical method (details provided in Sup plementary Information). The colloidal solutions obtained were cast on TEM grids and dried. From the TEM images of the silica-coated AgPRs, some of which were vertically-oriented with respect to the grid surface, the thicknesses of both of the SAgPRs and LAgPRs were estimated to be 10 ± 1 nm (Figure S1). Therefore, the aspect ratios of the SAgPRs and the LAgPRs were approximately 2.7 and 4.4, respectively.

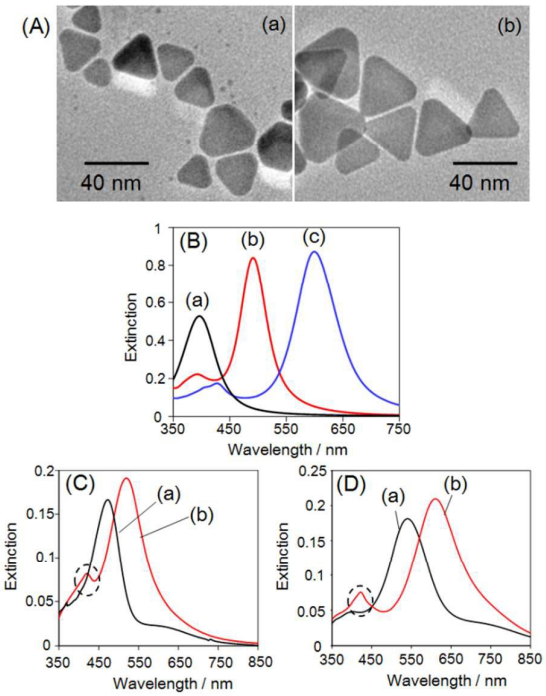

Figure 1. (A) TEM images for AgPRs, synthesized by irradiation with LED of center wavelengths of (a) 470 (SAgPRs) and (b) 550 nm (LAgPRs). (B) Extinction spectra for colloidal aqueous solutions of (a) spherical silver nanoparticles as a seed, (b)SAgPRs, and (c) LAgPRs. (C) Extinction spectra for (a) SAgPRs/ITO and (b) TCPP/SAgPRs/ITO. (D) Extinction spectra for (a) LAgPRs/ITO and (b) TCPP/LAgPRs/ITO.

Next, in order to investigate the optical properties, the extinction spectra of colloidal solutions of the AgPRs were measured. As shown in Figure 1(B), the SAgPRs and LAgPRs showed a clear extinction peak in the visible region (at approximately 490 and 600 nm, respectively). These peaks, which appeared at longer wavelengths than that of the colloidal solution of Ag nanospheres, were ascribed to the in-plane dipole mode of the AgPRs.[43,44] The LSPR wavelength of the mode from the SAgPRs was shorter than that from the LAgPRs because the aspect ratio of SAgPRs was smaller than that of LAgPRs.[28]

3.2. Characterization of the photoelectric conversion systems consisting of AgPRs and TCPP

The plasmonic photoelectric conversion systems comprising the AgPRs-TCPP hybrids were fabricated by the layer-by-layer assembly methods as described in experimental section. The zeta potential for the SAgPRs and LAgPRs dispersed in the aqueous phase was measured to be -14.2 ± 0.8 mV and -16.8 ± 2.2 mV, respectively. The occurrence of these negative potentials is surely attributed to be the presence of the citric acids protecting the AgPRs. Therefore, it is reasonable that the AgPRs with the negative potentials were immobilized onto the ITO electrode surface by the electrostatic absorption. In this study, the composite layers of the MHA SAMs and Ti(O) were

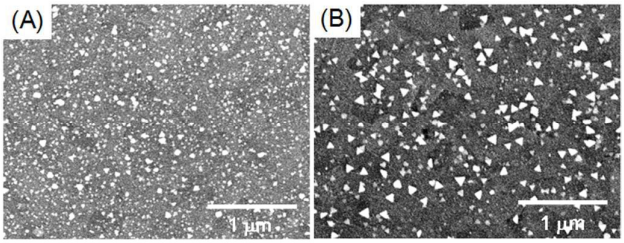

Figure 2. SEM images of (A) SAgPRs/ITO and (B) LAgPRs/ITO.

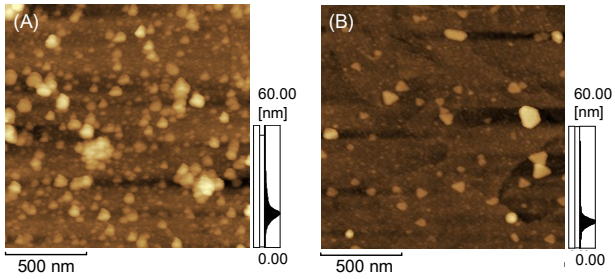

Figure 3. AFM images of the ITO electrodes modified with (A) SAgPRs and (B) LAgPRs.

adopted as linking layers for the TCPP modification. The thickness of MHA SAMs immobilized on the AgPRs by the self-assembling process can be estimated to be between 2.0 and 2.5 nm as in previous reports.[45,46] The thickness of Ti(O) linking layer is estimated to be approximately 0.36 nm from our previous report.[47] Therefore, the distance between TCPP molecules and AgPR surfaces is expected to be less 3 nm. The LSPR peak from the AgPRs changed during the fabrication processes. While the LSPR peaks of the SAgPRs/ITO and LAgPRs/ITO were generated at 478 nm and 545 nm, respectively, those after the modification of TCPP were red-shifted to 527 and 619 nm [Figure 1(C) and (D)]. The generating wavelength of the LSPR peak from AgPRs is very sensitive to changes in the refractive index (RI) of the surrounding medium.[28] Therefore, it is reasonable to assume that the changes in the LSPR peaks were due to the increases in the RI around the AgPRs caused by the modification of the molecular layers (MHA-SAMs, Ti(O), and TCPP). The magnitude of the shift was larger for the TCPP/LAgPRs/ITO than for the TCPP/SAgPRs/ITO. A previous report for AgPRs demonstrated that the higher aspect ratio leads to higher RI susceptibility of the LSPR peak.[28] It is therefore reasonable to consider that the difference in the RI susceptibility between the AgPRs in this study can be ascribed to the difference in the aspect ratio of the SAgPRs (2.7) and the LAgPRs (4.4). In addition, both the TCPP/SAgPRs/ITO and TCPP/LAgPRs/ITO showed a weak peak around 425 nm (indicated by the dashed circle in the spectra), indicating that the TCPP molecules were immobilized on the electrodes because the peak position is similar to that of the Soret band of TCPP (418 nm in ethanol solution). From the SEM images (Figure 2) and the absence of coupling modes between the LSPRs from the AgPRs [Figure 1(C) and 1(D)], it was concluded that the AgPRs were well-dispersed on the electrodes. From the AFM images (Figure 3), the triangular nanoplates on the ITO electrode surfaces were frequently observed. Also, the thicknesses of the nanoplates were 13.8 ± 1.2 nm and 13.7 ± 1.4 nm for SAgPRs/ITO and LAgPRs/ITO, respectively, almost the same as that of the AgPRs estimated from the TEM images (Figure S1). Therefore, the faces of the SAgPRs and LAgPRs were mostly parallel to the ITO surface. The coverage (θ_{AgPR}) of the SAgPRs and LAgPRs on the ITO electrodes estimated using the ImageJ software were 0.28 and 0.27, respectively.[48]

The number of TCPP molecules immobilized on each of the SAgPRs/ITO and the LAgPRs/ITO was estimated by immersing the electrode in 3 mL of a 0.2 M aqueous solution of NaOH for 10 min to extract the surface-immobilized TCPP into the solution. It was confirmed that all the TCPP molecules were removed from the electrodes by this treatment by the disappearance of the absorption peak of the Soret band from the sample electrode. The density of TCPP molecules (d_{TCPP} mol/cm^2) on the SAgPRs/ITO and the LAgPRs/ITO were calculated from the absorption spectra of the extract solution to be 4.8×10^{-10} and 2.9×10^{-10} mol/cm^2, respectively. When TCPP molecules were immobilized on the ITO electrode after the modification process of Ti(O) layers but without the AgPRs, the density of molecules immobilized was only ~6.9×10^{-11} mol/cm^2. Therefore, by substituting in ($[d_{TCPP} - \{6.9 \times 10^{-11} \times (1 - \theta_{AgPR})\}]/d_{TCPP}$), it was estimated that 90 and 83 % of TCPP molecules on TCPP/SAgPRs/ITO and TCPP/LAgPRs/ITO were immobilized on the surfaces of the SAgPRs and LAgPRs, respectively.

3.3. Effect of LSPR excitation of AgPRs on photoelectric conversion properties

Figure 4(A) shows the photocurrent action spectra from the TCPP/(SAgPRs, LAgPRs, and AgP)/ITO as a function of excitation wavelength, which were evaluated from the photocurrent densities at E = 0 V *vs*. Ag|AgCl. It can be concluded that the obtained photocurrents were mostly derived from the photo-excitation of TCPP molecules because (i) the currents generated by the electrodes without TCPP but otherwise identical were negligibly small (Figure S2) and (ii) the shape of the action spectra were similar to that of the absorption spectrum of TCPP (Figure 4(B)). From the results, it is seen that the photocurrents from both the TCPP/(SAgPRs and LAgPRs)/ITO were significantly larger than those from TCPP/AgP/ITO. In addition, in order to accurately evaluate the effect of the LSPRs on the photocurrent generation, the photocurrent obtained at each wavelength was corrected with the difference in the number of the TCPP molecules immobilized on the (SAgPRs, LSgPRs, and AgP)/ITO. The density of TCPP molecules in the TCPP/SAgPRs/ITO, and TCPP/LAgPRs/ITO were 4.8×10^{-10} and 2.9×10^{-10} mol/cm^2, respectively, as described above. The density on the AgP/ITO was estimated to be 4.0×10^{-10} mol/cm^2 by the same

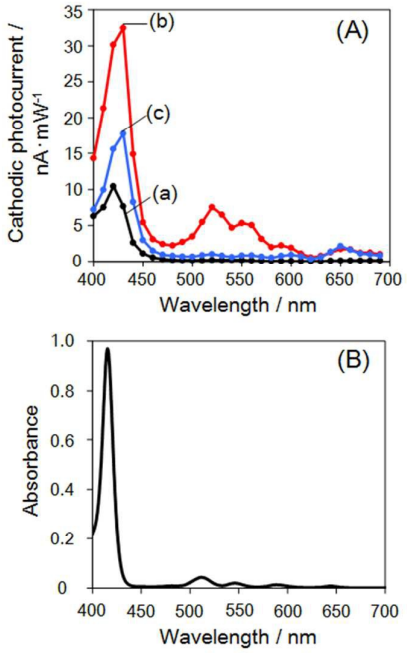

Figure 4. (A) Photocurrent action spectra for (a) TCPP/AgP/ITO, (b) TCPP/SAgPRs/ITO, (c) TCPP/LAgPRs/ITO after subtraction of the photocurrents of Ti(O)-modified AgP/ITO, SAgPRs/ITO, and LAgPRs/ITO, repectively. (B) Absorption spectrum of the ethanol solution of TCPP.

procedure as for the TCPP/AgPRs/ITO. The corrected action spectra are shown in Figure 5(A) (the magnified view at the Q-band region is shown in Figure 5(B)). The enhancement factors (EFs) of the photocurrents for TCPP/(SAgPRs and LAgPRs)/ITO against TCPP/AgP/ITO were calculated by dividing the photocurrent generated from the former by that from the latter at each wavelength. As shown in the plots of EFs (Figure 5(C)), the TCPP/SAgPRs/ITO and TCPP/LAgPRs/ITO have large EFs in the wavelength regions of 460–610 nm and 610–690 nm in the Q-bands region, respectively. The region of the photocurrent enhancements for TCPP/(SAgPRs and LAgPRs)/ITO agreed well with their LSPR bands in an aqueous electrolyte solution [see red- and blue-shaded regions in Figures 5(C) and (D)]. Note that the LSPR band positions are shifted in the aqueous environment from those in air as shown in Figure 1(C) and 1(D) due to different refractive indices [Figure 5(D)].[28] The maximum EFs for the photocurrent from TCPP/(SAgPRs and LAgPRs)/ITO were 37 at 560 nm and 35 at 610 nm, respectively. Teranishi *et al.* reported that the spectroscopic properties of the porphyrin change due to the electronic interaction between the π system of the porphyrin and the Au nanoparticles when the porphyrin and the Au nanoparticle is very close.[49-51] The effect is already small when the porphyrin and the Au nanoparticle is separated by bis(methylene) groups. In the present system, such a strong interaction of porphyrin π system and the Ag surface is unlikely because the TCPP molecules are separated from the Ag surface by MHA (C_{18}) as well as a Ti(O) layer. The observed photocurrent action spectra as well as the fluorescence excitation spectra (as described in section 3.4.) which match well with the Soret and the Q-bands of porphyrin further support that the electronic structure of TCPP is maintained in the state of being immobilized on AgPRs in the present case.

In this study, we succeeded in enhancing the photocurrents in both the shorter and longer wavelength regions in the Q-band, including the region where Au LSPR could not cause enhancement. Successful examples of efficient photocurrent enhancement utilizing Ag LSPR are few; the highest reported EF by the Ag LSPRs was 10.[17-19] This might be because the handling of Ag nanoparticles is difficult and/or because Ag nanoparticles are photochemically unstable possibly due to photocorrosion.[17,19,23] Also, the choice of Ag nanoparticle shape is important because the intensity of the local electric fields largely depends on their shapes. In this study, we succeeded in efficiently enhancing the photocurrents by up to 37 times. The positive results might well be due to the choice of the AgPRs, which generate strong local electromagnetic fields as shown in section 3.4 and the fabrication of systems stable upon photoirradiation as described in section 3.6.

3.4. Mechanism of photocurrent enhancement

As stated in the previous section, the photocurrents of TCPP immobilized on the AgPRs/ITO were enhanced at the specific wavelength region where their LSPR bands reside. As a result, the photocurrent intensity showed the following features:

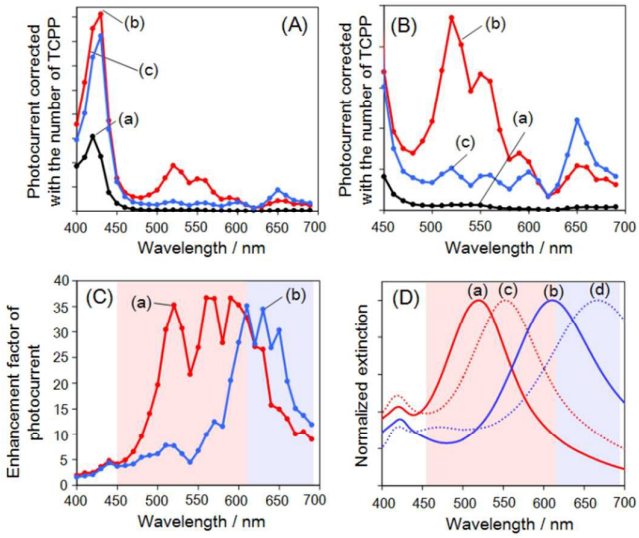

Figure 5. (A) Photocurrent action spectra corrected with the number of TCPP for (a) TCPP/AgP/ITO, (b) TCPP/SAgPRs/ITO, and (c) TCPP/LAgPRs/ITO. (B) Magnified view of (A) at the Q-band region. (C) EFs of photocurrents of (a) TCPP/SAgPRs/ITO and (b) TCPP/LAgPRs/ITO against TCPP/AgP/ITO. (D) Normalized extinction spectra for (a) TCPP/SAgPRs/ITO and (b) TCPP/LAgPRs/ITO in air and (c) TCPP/SAgPRs/ITO and (d) TCPP/LAgPRs/ITO in electrolyte aqueous solution. Red-shaded and blue-shaded areas indicate the wavelength regions where the photocurrent enhancements for TCPP/SAgPRs/ITO and TCPP/LAgPRs/ITO were, respectively, dominant.

TCPP/SAgPRs/ITO > TCPP/LAgPRs/ITO below 610 nm and TCPP/LAgPRs/ITO > TCPP/SAgPRs/ITO above 610 nm. It has recently been reported that the LSPR from AgPRs led to enhancement of emission of fluorophores.[52,53] To shed light into the mechanism of the photocurrent, we investigated the fluorescence enhancement by the AgPRs. Figure 6(A) shows the fluorescence excitation spectra monitored at 715 nm for the electrodes corrected with the difference in the number of the TCPP molecules on each of the electrodes. The enhancement of fluorescence of the fluorophores by the LSPR excitation can be explained by two mechanisms:[54,55] photoexcitation enhancement, which is induced when the LSPR band overlaps with the absorption band of the fluorophores, and the enhancement in the radiative decay rate from the photoexcited state, which is induced when the LSPR band overlaps with the emission band. In the present case, the photoexcitation enhancement would be very small when excited at the Soret band at 423 nm because the band is far away from the in-plane dipole LSPR modes (main LSPR modes) of both of the AgPRs. Thus, the larger enhancement of fluorescence at 715 nm when excited at 423 nm for TCPP/LAgPRs/ITO than that for TCPP/SAgPRs/ITO can be mostly ascribed to a larger decay rate enhancement for the former, which is reasonable because the fluorescence wavelength is well overlapped with the LSPR band of TCPP/LAgPRs/ITO rather than that of TCPP/SAgPRs/ITO. This

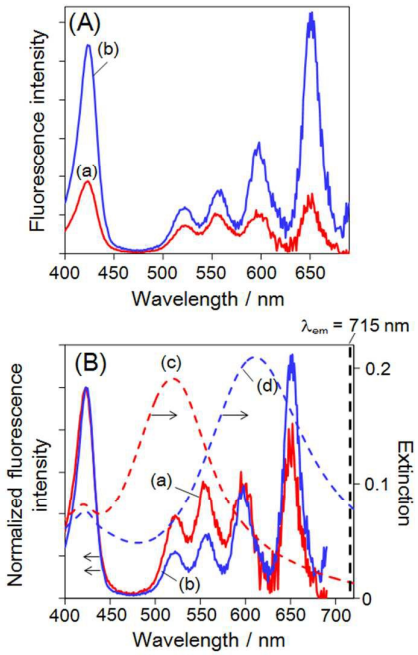

Figure 6. (A) Fluorescence excitation spectra (λ_{em} = 715 nm) per TCPP molecule for (a) TCPP/SAgPRs/ITO and (b) TCPP/LAgPRs/ITO. (B) Fluorescence excitation spectra (λ_{em} = 715 nm) normalized at 423 nm for (a) TCPP/SAgPRs/ITO and (b) TCPP/LAgPRs/ITO, and extinction spectra for (c) TCPP/SAgPRs/ITO and (d) TCPP/LAgPRs/ITO. All spectra were measured in air.

suggests that we can extract the effect of the phtoexcitation enhancement if we subtract the effect of decay rate enhancement by normalizing the fluorescence intensities from the two systems with those obtained by excitation of the Soret band. Upon normalization of the fluorescence excitation spectra at 423 nm [Figure 6(B)], the fluorescence intensities were TCPP/SAgPRs/ITO > TCPP/LAgPRs/ITO when excited at 460–600 nm, where the LSPR band of TCPP/SAgPRs/ITO is prominent, whereas TCPP/LAgPRs/ITO > TCPP/SAgPRs/ITO when excited at above 600 nm, where the LSPR band of TCPP/LAgPRs/ITO is prominent. The excitation spectral shapes are similar to those displayed by the photocurrent action spectra [Figure 5(A) and (B)]. These results suggest that the wavelength-dependent switching of the trend in the photocurrents of TCPP/SAgPRs/ITO and TCPP/LAgPRs/ITO was the result of the wavelength-specific enhancement of the photoexcitation efficiency.

To further demonstrate that the enhancement of photocurrent is caused by the generation of strong local electromagnetic fields *via* the LSPR excitation of the AgPRs, we estimated the electric field distributions at the points 1 nm away from the AgPR surfaces in water using FDTD simulation at the excitation wavelength of 520, 560, 600, and 650 nm, corresponding to the peak of the Q-band. The geometric models (Figure S3) of the SAgPRs and LAgPRs for the simulation were obtained from the TEM images shown in Figures 1(A) and S1. As shown in Figure 7(A), the electromagnetic field strengths ($|E/E_0|^2$, normalized by the incident light power) and the spatial position of the maximum electromagnetic fields are dependent on the excitation wavelength and the size of the AgPRs.

The SAgPRs and the LAgPRs showed the highest local fields at a shorter (around 560 nm) and a longer wavelength region (around 650 nm), respectively, in the Q-band region (Figure 7(B)). The obtained field intensities are substantially different from those reported in previous papers.[56,57] This may be due to the difference in the shape of the models (*e.g.* roundness of the corner). In addition, those strong electromagnetic fields are well distributed over the AgPR faces, and therefore should be strongly contributed to the excitation of TCPP on the AgPRs. These wavelength dependences of the intensity of the local electromagnetic fields from the SAgPRs and LAgPRs are well-correlated with those of the EFs of the photocurrents from the TCPP/SAgPRs/ITO and TCPP/LAgPRs/ITO, respectively. As a consequence, it is concluded from these results that the photocurrent enhancements were induced by the LSPR excitation of the AgPRs.

3.5. Photocurrent enhancement over the Q-band region of porphyrin

Although we succeeded in controlling the wavelength region at which the photocurrents of TCPP are enhanced, it has also become evident that single plasmonic nanoparticles alone cannot enhance the photocurrent over the entire Q-band wavelength region. Therefore, we attempted to achieve the photocurrent enhancement over the entire Q-band region by

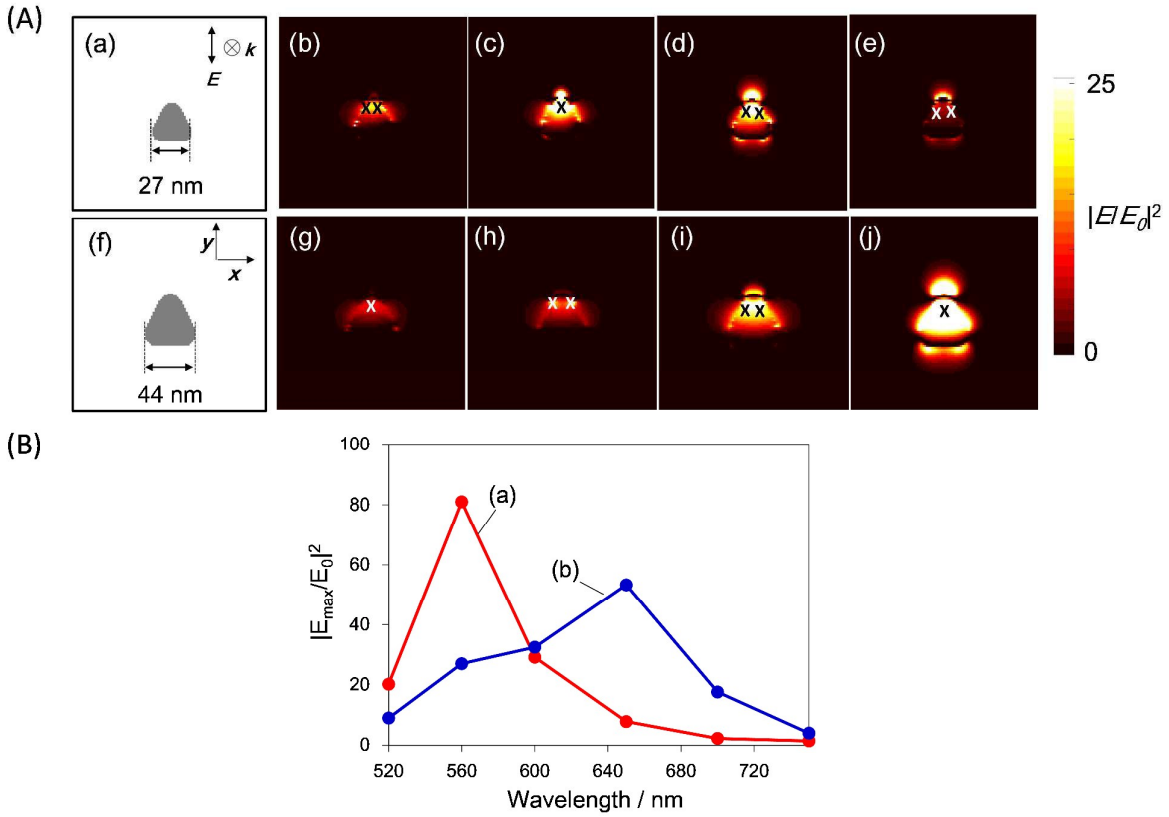

Figure 7. (A) Electromagnetic field distributions of SAgPRs (edge length: 27 nm, aspect ratio: 2.7) and LAgPRs (edge length: 44 nm, aspect ratio: 4.4) in water (n = 1.333). The geometric front views of SAgPR (a) and LAgPR (f), and their electromagnetic field distributions at the wavelength of 520 nm ((b), (g)), 560 nm ((c), (h)), 600 nm ((d), (i)), and 650 nm ((e), (j)), at the point 1 nm distance above the surfaces of SAgPR and LAgPR. The field strengths were normalized by the incident electromagnetic field strength. The area in white color means $|E/E_0|^2 \geq 25$. The spatial position of the maximum electromagnetic field is shown by X. (B) Maximum intensity of the electromagnetic field (corresponding to position X indicated in (A)) generated on the (a) SAgPRs and (b) LAgPRs with excitation at the peaks of the Q-band and at 700 and 750 nm. Electromagnetic field distributions at each of the wavelengths extended to 750 nm are shown in Figure S4.

the use of a combination of AgPRs with different aspect ratios, which generate the LSPR at different wavelengths. As shown in Figure 8(A), TCPP/MAgPRs/ITO in the electrolyte solution showed an LSPR band containing two extinction peaks (548 and 676 nm) derived from the in-plane dipole mode of the SAgPRs and LAgPRs over a wide region. The photocurrent action spectra corrected for the difference in the number of TCPP molecules of the TCPP/MAgPRs/ITO and TCPP/AgP/ITO as a reference electrode are shown in Figure 8(A) (and magnified view: Figure 8(B), the photocurrents before correction are shown in Figure S5). In Figure 8(C), the EFs of the photocurrent at each wavelength from the electrode against TCPP/AgP/ITO are shown. Interestingly, the maximum EF value was approximately 41 at a wavelength of 620 nm. As shown in Figure S6, the excellent EFs were observed mostly between those of TCPP/SAgPRs/ITO and TCPP/LAgPRs/ITO, covering the entire visible region (460-690 nm). These results show that the photocurrents of TCPP were effectively enhanced over the wide Q-band region by expanding the generating wavelength of Ag LSPR.

3.6 Photocurrent enhancement by broadband LSPR excitation and stability of the photocurrent generation

The simultaneous use of two kinds of the AgPRs led to the photocurrent enhancement over the entire Q-band region, as shown in the above experiments using monochromatic excitation light. In order to demonstrate the usability of this technique, we also evaluated the photocurrent enhancement by the standard AM1.5G sunlight (150 mW/cm^2). Light above 480 nm was passed through a longpass filter (of 480 nm) to extract the enhancement at the Q-band region (480-690 nm) where the LSPR is prominent. The photocurrent values corrected for the number of immobilized TCPP are shown in Figure 9. All of the sample electrodes containing the AgPRs efficiently generated larger photocurrents than the TCPP/AgP/ITO. The average EFs were 19, 14, and 21 for TCPP/SAgPRs, LAgPRs, and MAgPRs/ITO, respectively. The photocurrent generated from the TCPP/SAgPRs/ITO was

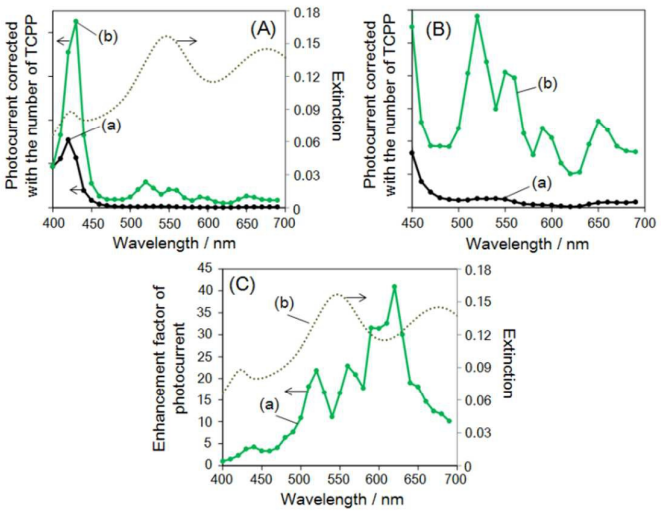

Figure 8. (A) Photocurrent action spectra corrected with the number of TCPP for (a) TCPP/AgP/ITO [the same as (a) in Figure 3(A)] and (b) TCPP/MAgPRs/ITO. (B) Magnified view of (A) at the Q-band region. (C) Photocurrent EFs of TCPP/MAgPRs/ITO against TCPP/AgP/ITO and (b) an extinction spectrum measured in aqueous electrolyte solution for TCPP/MAgPRs/ITO.

greater than that from the TCPP/LAgPRs/ITO, because the LSPR band of the TCPP/SAgPRs/ITO matches better with the Q-band of TCPP as compared with the TCPP/LAgPRs/ITO. In addition, the photocurrent from TCPP/MAgPRs/ITO was even larger than that from TCPP/SAgPRs/ITO. These results show the effectiveness of using a combination of different plasmonic nanoparticles.

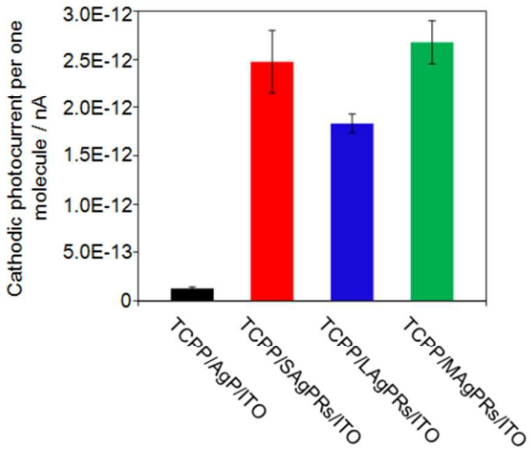

Figure 9. Photocurrent values of TCPP/AgP/ITO, TCPP/SAgPRs/ITO, TCPP/LAgPRs/ITO, and TCPP/MAgPRs/ITO generated by irradiation of AM1.5G sunlight through the longpass filter of 480 nm. Error bars were obtained by measuring the photocurrent thrice.

Finally, we examined the photostability of the fabricated systems based on the AgPRs. Figure 10 shows the photocurrent profile of the TCPP/MAgPRs/ITO, upon the sequential on/off switching of AM 1.5G irradiation, through the longpass filter for 10 min. The photocurrent was stably generated without any decrease in the current density over the measurement period. This result indicates that the photoelectric conversion systems based on the Ag nanoparticles fabricated in this study possess reasonable photostability. Previous paper reported that the spherical Ag nanoparticles protected with aliphatic molecules were stable during the photocurrent measurements.[17] In our systems, the AgPRs were modified with the long alkylcarboxylates (MHA) in the immobilization process of TCPP. Thus, the modification of the aliphatic molecules may prevent the photocorrosion of even the anisotropic nanoparticles, which contain larger curvature than spherical Ag nanoparticles.

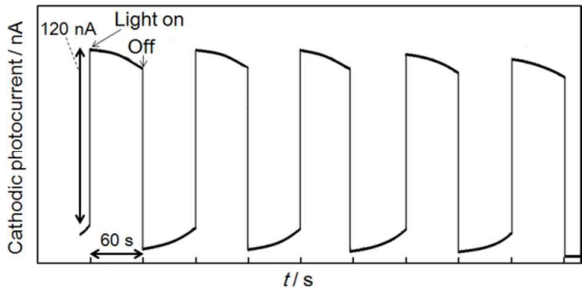

Figure 10. Photocurrent profile of TCPP/MAgPRs/ITO by irradiation of AM1.5G sunlight through the longpass filter of 480 nm upon sequential on/off light switching for 10 min.

4. Conclusion

In this study, photoelectric conversion systems consisting of the TCPP molecules and the two kinds of AgPRs (with different aspect ratios) were fabricated. The incorporation of the AgPRs led to an enhancement of photocurrent because of efficient photoexcitation of TCPP at wavelengths that were tuned by adjusting the aspect ratio. The maximum EFs for the SAgPRs and LAgPRs were 37 and 35, respectively. Next, we succeeded in enhancing the photocurrent over the wide Q-bands region with a maximum EF of 41 by the combined use of SAgPRs and LAgPRs. The control and expansion technique of these Ag LSPR bands with high photostability has potential for application in plasmonic photoelectrochemical devices such as artificial photosynthetic systems and photoelectrochemical biosensors. Furthermore, combination of various other plasmonic materials could lead to the development of high-performance plasmonic devices.

Acknowledgements

This work was supported in part by Grant-in-Aid for Young Scientists B (Grant No. 26810102) from JSPS KAKENHI and Applied Research Grant from Nihon University.

Notes and references

(1) B. O'Regan and M. Grätzel, *Nature*, 1991, **353**, 737-740.
(2) H. Imahori and S. Fukuzumi *Adv. Funct. Mater.*, 2004, **14**, 525-536.
(3) A. Okamoto, T. Kamei and I. Saito, *J. Am. Chem. Soc.*, 2006, **128**, 658-662.
(4) Y. Shinozaki, G. Richards, K. Ogawa, A. Yamano, K. Ohara, K. Yamaguchi, S. Kawano, K. Tanaka, Y. Araki, T. Wada and J. Otsuki, *J. Am. Chem. Soc.*, 2013, **135**, 5262–5265.
(5) J. Otsuki, *Supramolecular Energy and Electron-Transfer Processes and Their Switching, in Multiporphyrin Arrays, Fundamentals and Applications*, ed. D. Kim, Pan Stanford, USA, 2012, 587–628.
(6) M. Gouterman, *J. Mol. Spec.* 1961, **6**, 138-163.
(7) H. Imahori, H. Norieda, H. Yamada, Y. Nishimura, I. Yamazaki, Y. Sakata and S. Fukuzumi, *J. Am. Chem. Soc.*, 2001, **123**, 100-110.
(8) C. Y. Lee and J. T. Hupp, *Langmuir*, 2010, **26**, 3760-3765.
(9) T. Akiyama, M. Nakada, N. Terasaki and S. Yamada, *Chem. Commun.*, 2006, 395-397.
(10) T. Akiyama, K. Aiba, K. Hoashi, M. Wang, K. Sugawa and S. Yamada, *Chem. Commun.*, 2010, **46**, 306-308.
(11) K. Sugawa, T. Akiyama, H. Kawazumi and S. Yamada, *Langmuir*, 2009, **25**, 3887-3893.
(12) K. Sugawa, S. Hirono, T. Akiyama and S. Yamada, *Photochem. Photobiol. Sci.*, 2012, **11**, 318-322.
(13) C. Kong, G. Zhang, Y. Li, D. Li and Y. Long, *RSC Adv.*, 2013, **3**, 3503-3507.
(14) H. Nagatani, S. Tonari, T. Shibata and T. Sagara, *Electrochem. Commun.*, 2011, **13**, 985-988.
(15) K. Ikeda, K. Takahashi, T. Masuda and K. Uosaki, *Angew. Chem. Int. Ed.*, 2011, **50**, 1280-1284.
(16) T. Arakawa, T. Munaoka, T. Akiyama and S. Yamada, *J. Phys. Chem. C*, 2009, **113**, 11830-11835.
(17) K. Kanaizuka, S. Yagyu, M. Ishizaki, H. Kon and T. Togashi, *Appl. Phys. Lett.*, 2012, **101**, 063103-1-063103-4.
(18) R. Matsumoto, H. Yonemura and S. Yamada, *J. Phys. Chem. C*, 2013, **117**, 2486-2493.
(19) S. D. Standridge, G. C. Schatz and J. T. Hupp, *J. Am. Chem. Soc.*, 2009, **131**, 8407-8409.
(20) T. Kawasaki, Y. Takahashi and T. Tatsuma, *J. Phys. Chem. C*, 2013, **117**, 5901-5907.
(21) K. Ikeda, K. Takahashi, T. Masuda, H. Kobori, M. Kanehara, T. Teranishi and K. Uosaki, *J. Phys. Chem. C*, 2012, **116**, 20806-20811.
(22) S. G. Yenchalwar, R. R. Devarapalli, A. B. Deshmukh and M. V. Shelke, *Chem. Euro. J.*, 2014, **20**, 7402-7409.
(23) N. C. Jeong, C. Prasittichai and J. T. Hupp, *Langmuir*, 2011, **27**, 14609-14614.
(24) E. J. Zeman and G. C. Schatz, *J. Phys. Chem.*, 1987, **91**, 634-643.
(25) K. Tanabe, *J. Phys. Chem. C*, 2008, **112**, 15721-15728.
(26) J. M. McMahon, S. Li, L. K. Ausman and G. C. Schatz, *J. Phys. Chem. C*, 2012, **116**, 1627-1637.
(27) E. Hao and G. C. Schatz, *J. Chem. Phys.*, 2004, **120**, 357.
(28) D. E. Charles, D. Aherne, M. Gara, D. M. Ledwith, Y. K. Gun'ko, J. M. Kelly, W. J. Blau and M. E. Brennan-Fournet, *ACS Nano*, 2010, **4**, 55-64.
(29) M. Salvador, B. A. MacLeod, A. Hess, A. P. Kulkarni, K. Munechika, J. I. L. Chen and D. S. Ginger, *ACS Nano*, 2012, **6**, 10024-10032.
(30) M. M. Shahjamali, M. Salvador, M. Bosman, D. S. Ginger and C. Xue, *J. Phys. Chem. C*, 2014, **118**, 12459-12468.
(31) M. Stavytska-Barba, M. Salvador, A. Kulkarni, D. S. Ginger and A. M. Kelley, *J. Phys. Chem. C*, 2011, **115**, 20788-20794.
(32) A. P. Kulkarni, K. M. Noone, K. Munechika, S. R. Guyer and D. S. Ginger, *Nano Lett.*, 2010, **10**, 1501-1505.
(33) D. U. Karatay, M. Salvador, K. Yao, A. K.-Y. Jen and D. S. Ginger, *Appl. Phys. Lett.*, 2014, **105**, 033304.
(34) K. Yao, M. Salvador, C.-C. Chueh, X.-K. Xin, Y.-X. Xu, D. W. deQuilettes, T. Hu, Y. Chen, D. S. Ginger and A. K.-Y. Jen, *Adv. Energy Mater.*, 2014, **4**, 1400206.
(35) C. Xue and C. A. Mirkin, *Angew. Chem. Int. Ed.,* 2007, **46**, 2036-2038.
(36) A, Callegari, D. Tonti and M. Chergui, *Nano Lett.*, 2003, **3**, 1565-1568.
(37) K. G. Stamplecoskie and J. C. Scaiano, *J. Am. Chem. Soc.*, 2010, **132**, 1825-1827.
(38) W. Wang, S. Efrima and O. Regev, *Langmuir*, 1998, **14**, 602-610.
(39) J. C. Azcárate, G. Corthey, E. Pensa, C. Vericat, M. H. Fonticelli, R. C. Salvarezza and P. Carro, *J. Phys. Chem. Lett.*, 2013, **4**, 3127-3138.
(40) T. Akiyama, A. Miyazaki, M. Sutoh, I. Ichinose, T. Kunitake and S. Yamada, *Colloids Surf. A*, 2000, **169**, 137-141.
(41) K. Araki, D. Yang, T. Wang, R. Selyanchyn, S. Lee and T. Kunitake, *Anal. Chim. Acta*, 2013, **779**, 72-81.
(42) A. D. Rakic, A. B. Djurisic, J. M. Elazar and M. L. Majewski, *Appl. Opt.*, 1998, **37**, 5271-5287.
(43) R. Jin, Y. C. Cao, C. A. Mirkin, K. L. Kelly, G. C. Schatz and J. G. Zheng, *Science*, 2001, **294**, 1901-1903.
(44) R. Jin, Y. C. Cao, E. Hao, G. S. Métraux, G. C. Schatz and C. A. Mirkin, *Nature*, 2003, **425**, 487-490.
(45) S. Techane, D. R. Baer and D. G. Castner, *Anal. Chem.*, 2011, **83**, 6704–6712.
(46) J. Lahann, S. Mitragotri, T.-N. Tran, H. Kaido, J. Sundaram, I. S. Choi, S. Hoffer, G. A. Somorjai and R. Langer, *Science*, 2003, **299**, 371–374.
(47) K. Sugawa, T. Tamura, H. Tahara, D. Yamaguchi, T. Akiyama, J. Otsuki, Y. Kusaka, N. Fukuda and H. Ushijima, *ACS Nano*, 2013, **7**, 9997-10010.
(48) C. A. Schneider, W. S. Rasband and K. W. Eliceiri, *Nat. Methods*, 2012, **9**, 671-675.
(49) M. Kanehara, H. Takahashi and T. Teranishi, *Angew. Chem. Int. Ed.*, 2008, **47**, 307-310.

(50) M. Sakamoto, D. Tanaka, H. Tsunoyama, T. Tsukuda, Y. Minagawa, Y. Majima and T. Teranishi, *J. Am. Chem. Soc.*, 2012, **134**, 816-819.
(51) D. Tanaka, Y. Inuta, M. Sakamoto, A. Furube, M. Haruta, Y.-G. So, K. Kimoto, I. Hamada and T. Teranishi, *Chem. Sci.*, 2014, **5**, 2007-2010.
(52) K. Munechika, Y. Chen, A. F. Tillack, A. P. Kulkarni, I. J.-L. Plante, A. M. Munro and D. S. Ginger, *Nano Lett.*, 2010, **10**, 2598-2603.
(53) K. Munechika, Y. Chen, A. F. Tillack, A. P. Kulkarni, I. J.-L. Plante, A. M. Munro and D. S. Ginger, *Nano Lett.*, 2011, **11**, 2725-2730.
(54) J. R. Lakowicz, *Anal. Biochem.*, 2001, **298**, 1–24.
(55) F. Xie, M. S. Baker and E. M. Goldys, *Chem. Mater.*, 2008, **20**, 1788–1797.
(56) K. L. Kelly, E. Coronado, L. L. Zhao and G. C. Schatz, *J. Phys. Chem. B*, 2003, **107**, 668-677.
(57) E. Hao and G. C. Schatz, *J. Chem. Phys.*, 2004, **120**, 357-366.